scientific reports

OPEN

Loss of Kat2b impairs intraflagellar transport and the Hedgehog signaling pathway in primary cilia

Jae Hee Jun[1,3], Hwayeon Cha[1,3], Je Yeong Ko[1], Ho-Shik Kim[2], Kyung Hyun Yoo[1✉] & Jong Hoon Park[1✉]

Primary cilia are sensory organelles that regulate various signaling pathways. When microtubules are compared to a highway, motor proteins carry and transport cargo proteins, which are tuned by post-translational modifications, such as acetylation. However, the role of acetylation in primary cilia regulation remains unclear. In this study, histone K (lysine) acetyltransferase 2 B (Kat2b) was identified as a novel regulator of primary cilia. Kat2b, which mainly regulates transcription as a p300/CBP associated factor, is localized to the cytosol, centrosome, and cilium basal body. In addition, basal Kat2b expression gradually increased during ciliogenesis. Kat2b regulates the rate of cilia assembly, particularly in the early stages, and loss of Kat2b reduces the recruitment of intraflagellar transport (IFT) components to the ciliary axoneme and impairs Hedgehog (Hh) signaling activation. In addition, Kat2b-knockout mice showed mild abnormalities and ciliary IFT defects in the kidneys. These results establish a link between acetylation regulated by Kat2b and its relevance to ciliary assembly and function.

Keywords Acetylation, Ciliogenesis, Intraflagellar transport, Kat2b, Primary cilia

The primary cilium, which is non-motile in kidney epithelial cells, is a rod-like cellular organelle that projects from the plasma membrane[1]. For decades, the primary cilium has been considered degenerate; however, it was recently reported that the loss of primary cilia causes disorders collectively known as primary ciliopathies[2]. Ciliopathy includes a wide range of diseases, such as polycystic kidney disease (PKD)[3], nephronophthisis (NPHP), Bardet-Biedl syndrome (BBS), and Joubert syndrome[4,5]. Moreover, it has been reported that cancer, obesity, and schizophrenia are related to primary cilia[6,7], which act as a cellular antenna for numerous biological signaling pathways, such as the Hedgehog (Hh), Notch, PCP, and mechanosensing pathways[8].

The primary cilia are composed of the basal body, transition zone, ciliary membrane, ciliary tip, and axoneme[9]. The axoneme is a microtubule-based ciliary backbone with a '9+0' arrangement—nine outer doublets and no central microtubules[10]. Components of cilium assembly and maintenance, such as intraflagellar transport (IFT) complex proteins and components for signal transmission, move along the ciliary backbone[11,12]. Since these proteins are not synthesized in primary cilia, smooth transport of IFT proteins is required for normal functioning within primary cilia[13]. Thus, microtubules work as a 'highway' for these ciliary proteins.

Microtubules are subjected to diverse post-translational modifications (PTMs), including acetylation, polyglutamylation, detyrosination/tyrosination, polyglycylation, and phosphorylation[14]. PTMs affect microtubule dynamics, organization, and interactions with other cellular components and process occurs in tubulin dimers, including α-tubulin and β-tubulin[15,16]. Above all, acetylation is most-studied tubulin modification and occurs at lysine 40 (K40) of α-tubulin and it affects the stability of microtubules, especially enriched in primary cilia[17]. As an acetyl transferases, α-tubulin-N-acetyltransferase (α-TAT1) highly regulated α-tubulin acetylation and thus it is needed for rapid ciliogenesis[18]. Conversely, histone deacetylase 6 (HDAC6) and sirtuin 2 (SIRT2) deacetylated microtubule. However, further research is needed to reveal how PTMs regulate the formation and function of primary cilia.

K(lysine)acetyltransferase 2b (Kat2b), also known as the p300/CBP-associated factor (PCAF), has been recognized as a histone acetyltransferase (HAT) that promotes transcriptional activation[19]. Recently, it was reported that HAT and HDAC in the cytosol play novel roles[20]. Furthermore, in primary cilia research, HDAC2 knockdown promotes cilium assembly[21], whereas HDAC6 overexpression induces rapid cilium disassembly[22].

[1]Department of Biological Science, Sookmyung Women's University, Seoul 04310, Republic of Korea. [2]Department of Biochemistry, College of Medicine, The Catholic University of Korea, Seoul 06591, Republic of Korea. [3]Jae Hee Jun and Hwayeon Cha have contributed equally to this work. ✉email: khryu@sookmyung.ac.kr; parkjh@sookmyung.ac.kr

However, whether acetyltransferases and deacetylases affect ciliary functions, such as IFT components or Hh signaling, remains poorly characterized. Therefore, this study explored the role of Kat2b in primary cilia.

In this study, Kat2b was found to be required for the initial stage of α-tubulin acetylation for primary cilia assembly within 6 h. Interestingly, Kat2b localization in the cytosol, centrosome, and basal body gradually increased during ciliary assembly. Additionally, Kat2b interacts with α-tubulin to regulate its acetylation level. Remarkably, Kat2b depletion caused defects in IFT component levels and activation of Hh signaling. In addition, Kat2b-knockout mice showed mild abnormalities related to primary cilia defects in the kidneys. Taken together, these findings highlight the novel role of Kat2b in the assembly and function of primary cilia.

Materials and methods
Cell culture
Mouse embryo fibroblast NIH/3T3 (CRL-1658TM, ATCC) cells obtained from the Korean Cell Line Bank were used in this study. NIH/3T3 cells were cultured in Dulbecco's modified Eagle's medium (DMEM) (LM 001-05; Welgene) supplemented with 10% fetal bovine serum (FBS) (#26140-079; Gibco) at 37 °C under 5% CO_2. All culture media were supplemented with 1% penicillin–streptomycin (LS 202-02; Welgene). To induce primary cilia assembly, the cells were incubated under serum starvation conditions with DMEM without FBS for 6–24 h.

Kat2b-knockout mice
Kat2b-knockout mice (C57BL/6)[23] were kindly provided by Dr. Ho-Shik Kim (Catholic University of Korea, Seoul, Republic of Korea). To perform genotyping, mouse genomic DNA was isolated after overnight digestion of the clipping toe obtained from mice about postnatal 10 days at 55 °C in lysis buffer containing proteinase K. Next day, the mixture was subjected to heat inactivation at 85 °C for 30 min. PCR was performed using the primers to distinguish wild-type Kat2b (Oligo F1; 5′-TTCTAGATCTGCCGGTGTCC-3′, Oligo F2; 5′-CTGCC AGACCCTGTTTACAC-3′) from Kat2b-knockout (Oligo F1; 5′-TCGCCTTCTTGACGAGTTCT-3′). In vivo experimental procedures were conducted with the review and approval of the IACUC at Sookmyung Women's University, Seoul, Republic of Korea. Kidney extraction was performed after cervical dislocation.

Mouse embryonic fibroblast (MEF) isolation and culture maintenance
To generate Kat2b MEF cells, pregnant female mice were sacrificed at the embryonal stage (E13.5–E15.5). The tail of each embryo was saved for genotyping. The embryonic body was minced for 3 min using a blade. Next, minced tissue was incubated for 30–40 min in the 37 °C incubator with 0.05% Trypsin–EDTA (LS015-01; Welgene). The mixture was harvested with the culture medium and centrifuged at 1500 rpm for 3 min. The supernatant was aspirated, and the pellet was resuspended and plated onto T75 cells with culture medium (DMEM supplemented with 10% FBS and 1% P/S).

Antibodies and drugs
The primary antibodies used and their dilutions for western blotting (WB), immunocytochemistry/immunofluorescence (ICC/IF), and immunoprecipitation (IP) were as follows: mouse anti-PCAF(Kat2b) (1:500–1:1000 for WB and IP) (sc-13124; Santa Cruz), rabbit anti-IFT20 (1:500–1:1000 for WB) (13615-1-AP; Proteintech), rabbit anti-IFT25 (1:500 for WB, 1:200 for ICC/IF) (15732-1-AP; Proteintech), rabbit anti-IFT46 (1:1000 for WB) (ab122422; Abcam), rabbit anti-IFT52 (1:1000 for WB, 1:500 for ICC/IF) (17534-1-AP; Proteintech), rabbit anti-IFT88 (1:1000 for WB) (sc-84318; Santa Cruz), rabbit anti-IFT140 (1:1000 for WB, 1:500 for ICC/IF) (17460-1-AP; Proteintech), rabbit anti-GLI1 (1:500 for WB) (#2534; Cell Signaling Technologies), mouse anti-SMO (1:50 for ICC/IF) (sc-166685; Santa Cruz), mouse anti-acetylated α-tubulin (1:1000 for WB and ICC/IF) (T6793; Sigma), rabbit anti-acetylated α-tubulin (1:1000 for WB) (#5335; Cell Signaling Technologies), mouse anti-gamma-tubulin (1:1000 for WB) (T6557; Sigma), mouse anti- α-tubulin (1:1000 for WB) (#3873; Cell Signaling Technologies), rabbit anti-Arl13b (1:500 for ICC) (#17711-1-AP; Proteintech) mouse anti-α-tubulin (for IP) (sc-5286; Santa Cruz), rabbit anti-pericentrin (1:1000 for WB and ICC/IF) (ab4448; Abcam), rabbit cytoskeletal actin antibody (1:14,000 used as loading control for WB) (A300-491A; Bethyl Laboratories), normal mouse anti-IgG (for IP) (12-371; EMD Millipore), and rabbit anti-Flag (1:2,000 for WB) (F7425; Sigma).

The secondary antibodies used were as follows: goat anti-mouse IgG (1:2500 for WB) (ADI-SAB-100J; Enzo Life Sciences), goat anti-rabbit IgG (1:2500 for WB) (ADI-SAB-300J; Enzo Life Sciences), anti-biotin HRP-linked antibody (1:2500 for WB) (7075S; Cell Signaling Technologies), and Alexa Fluor 488 goat anti-mouse (1:1000 for ICC/IF) (#A11029; Invitrogen). The drugs used in this study were as follows: Garcinol (kindly gifted by Dr. Ho-Shik Kim, The Catholic University of Korea) and SAG (ab142160; Abcam).

siRNA (small interfering RNA) transfection, short hairpin RNA (shRNA) transduction and reagent treatment
To regulate target gene expression using siRNA, cells were transiently transfected with 30 nM control siRNA (sc-37007; Santa Cruz) and PCAF siRNA (sc-36199; Santa Cruz) using Lipofectamine RNAiMAX transfection reagent (#13778150; Invitrogen). To perform establishing stable Kat2b knock-out NIH3T3, we used PCAF shRNA Plasmid (Santa cruz, sc-36199-SH) and Control shRNA Plasmid-A (Santa cruz,, sc-108060) as control cell line. Lentiviral particles were generated through HEK293T cells, which were then transduced into NIH3T3 cells and subcultured in medium containing 5ug/ml puromycin (Gibco, A1113803). Plasmid transfection into NIH/3T3 cells was performed using FuGENE® HD Transfection Reagent (Promega) according to the manufacturer's instructions.

Quantitative real-time PCR (qRT-PCR)

Messenger RNA (mRNA) was extracted from cells using the NucleoSpin® DNA/RNA/Protein kit (Macherey–Nagel), strictly according to the manufacturer's instructions. Briefly, 2 µg of mRNA used was reverse-transcribed to cDNA using M-MLV Reverse Transcriptase (M170B; Promega), RNasin® ribonuclease inhibitor (N211A; Promega), 100 nM oligo-dT (C1101; Promega), and 2.5 nM dNTP mixture (U1205, U1225, U1215, and U1235; Promega). qRT-PCR was performed using SYBR Green qPCR Master Mix (PB20.15-05; PCR Biosystem, London, UK) and LightCycler® 96 System (Roche).

Western blotting

Proteins were extracted from cells and kidney tissues using NucleoSpin® RNA/Protein kit (Macherey–Nagel) according to the manufacturer's instructions. The protein concentration was quantified using bicinchoninic acid (BCA) solution (B9643; Sigma) and copper (II) sulfate sodium (C2284; Sigma). The protein samples were then separated by gel electrophoresis and transferred onto polyvinylidene fluoride (PVDF) membranes (AE-6667-P; ATTO). The membranes were blocked in 5% skim milk in PBS with 0.1% Tween® 20 (PBST) at room temperature for 1 h and incubated with primary antibodies diluted in 1% skim milk in PBST at 4 °C overnight for probing. The following day, the membranes were washed three times with PBST. Next, the membranes were incubated with horseradish peroxidase-conjugated secondary antibodies at room temperature for 2 h. The membranes were then washed three times with PBST. Membranes were detected with the chemiluminescent reagent EzWestLumWe Plus (WSE-7120; ATTO) using LAS-3000, LAS-4000 (Fujifilm), and Amersham Imager 600 (GE Healthcare). Using NE-PER Nuclear and Cytoplasmic Extraction Kit (78,833; Thermo Scientific) to separate nucleus and cytosol and incubated at 100℃ after mixing 5X protein sample buffer and quantified protein. Whether the gels/blots complied with the digital image and integrity policies was verified. The original full-length blots are provided in the Supplementary Materials.

Immunocytochemistry/immunofluorescence (ICC/IF)

For fluorescence staining, cells grown on 18×18 mm coverslips were washed in PBS and fixed in 4% paraformaldehyde (PFA) at room temperature for 15 min. Alternatively, the cells were fixed in cold methanol at −20 °C for 5 min. After fixation, the cells were blocked and permeabilized with PBS containing 0.1% Triton X-100 and 1% bovine serum albumin (BSA). The coverslips were incubated with diluted primary antibodies at 4 °C overnight. Next, the coverslips were washed thrice with PBS, incubated with secondary antibodies for 2 h, and stained with DAPI for 5 min at room temperature. Subsequently, the coverslips were washed three times with PBS. Next, the coverslips were mounted using mounting solution (S3023; DAKO). For fluorescence staining of the paraffin-embedded tissues, the sections were deparaffinized and rehydrated in graded ethanol. Brog Decloaker RTU (Biocare Medical) was used for heat induced antigen retrieval and the paraffin-embedded sections were blocked for 1 h followed by primary antibody incubation at 4℃ overnight. After washing, the slides were incubated with fluorescence-conjugated secondary antibodies (Invitrogen) at room temperature for 2 h. Subsequently, the slides were washed three times with PBS and mounted using a mounting medium containing DAPI (H-1500; Vector Laboratories). Cells and tissues were imaged using a confocal microscope (LSM-700; Carl Zeiss at the Chronic and Metabolic Diseases Research Center, Sookmyung Women's University) and Zen software (Carl Zeiss).

Co-immunoprecipitation (Co-IP)

The NIH/3T3 cells were grown to confluence. Subsequently, the cells were treated with a serum-free medium for 6 h to induce early stage ciliogenesis. Cells were washed briefly in PBS and lysed in buffer containing as follows: 25 mM HEPES, 150 mM NaCl, 1 mM DTT, 0.5% Triton X-100, protease inhibitor (cOmplete™ Protease inhibitor cocktail, 11697498001; Roche), and phosphatase inhibitor (PhosSTOP™, 4906837001; Roche). The protein content was measured using the BCA method. Next, 500–1000 µg of proteins with PCAF (Kat2b) antibody or α-tubulin antibody or mouse IgG antibody were incubated in a rotator at 4 °C overnight. The next day, magnetic beads were added, and the mixtures were incubated on a rotator at 4 °C for 4 h. The samples were washed three times in wash buffer containing 150 mM NaCl, 50 mM Tris–Cl, protease inhibitors, and phosphatase inhibitors. Next, the samples were boiled at 98 °C for 5 min and analyzed by western blotting as described previously.

Statistical analysis

All experiments were independently repeated at least in triplicate. Statistical analyses were conducted using GraphPad Prism 5 software (GraphPad, USA). The data was analyzed by one-tailed or two-tailed Student's t-test and values are presented as the mean ± SD. *$P < 0.05$, **$P < 0.01$, ***$P < 0.001$, ****$P < 0.0001$, n.s., not significant. The graph in Fig. 1d was generated from the results of three independent experiments under the identical conditions. Among the transfected cells, the tagged Kat2b was classified according to whether it was located in the cytosol, centrosome, and basal body. The measured results were calculated as a ratio of the number of transfected cells and showed in a graph.

Ethics approval

The study was conducted in accordance with the ARRIVE guidelines. All experiments were conducted according to the protocols approved by the IACUC at Sookmyung Women's University, Seoul, Republic of Korea.

Results

Kat2b localized to the cytosol, centrosome, and basal body during cilia assembly

Previous studies have shown that serum withdrawal from the culture medium induces the formation of primary cilia[24]. To investigate the basal expression of Kat2b during cilium assembly, NIH/3T3 cells were exposed to
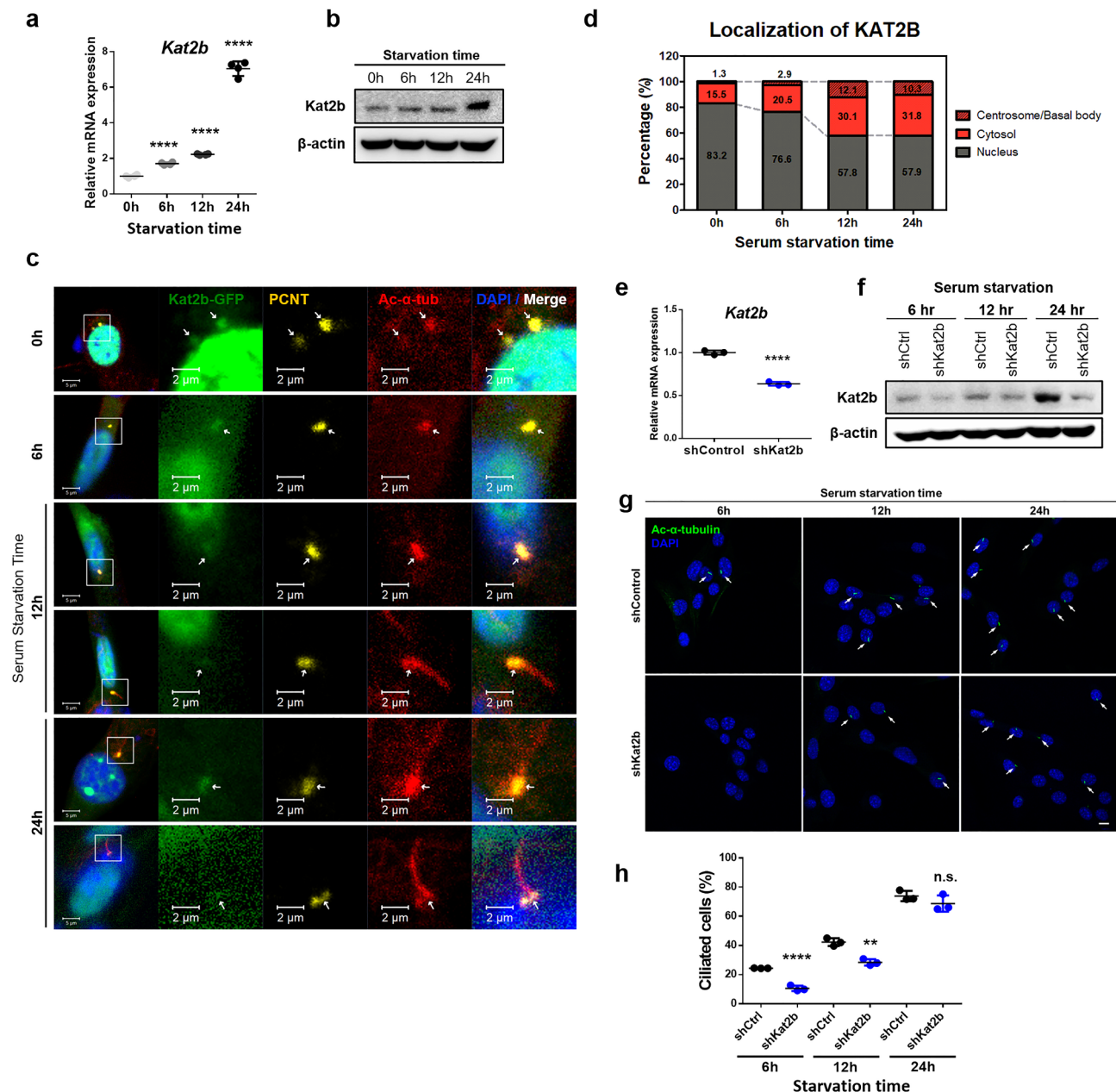
Fig. 1. The expression of Kat2b located in the cytosol, centrosome, and basal body increased during ciliogenesis, and depletion of Kat2b causes delays in ciliogenesis. (**a**) qRT-PCR data showing a gradual increase in the level of Kat2b transcript during primary cilia formation. (**b**) Western blot data showing an increase in Kat2b protein expression during ciliogenesis. (**c**) Representative figures of Kat2b localization in NIH/3T3 cells by serum starvation time (0 h, 6 h, 12 h, and 24 h). In serum starvation 12 h and 24 h, two panels were displayed depending on presence of primary cilia NIH/3T3 cells were transfected with expressing GFP-tagged full-length-Kat2b. After 24 h, cells were incubated under serum starvation conditions, followed by staining with endogenous acetylated α-tubulin for primary cilia (red) and pericentrin (PCNT) for centrosome and basal body (yellow). Nuclei were stained with DAPI (blue). (**d**) Quantification of the subcellular localization of Kat2b. Counted cell numbers were as follows: serum starvation for 6 h, n = 133; 12 h, n = 129; and 24 h, n = 124. Data were collected from three independent experiments. (**e**) Validation of transcriptional Kat2b level reduction in stable Kat2b knockdown NIH/3T3 cell line using qRT-PCR. (**f**) Validation of translational Kat2b level reduction in stable Kat2b KO-NIH3T3 cells or control KO-NIH3T3 using western blot analysis. (**g**) Representative figures of ciliated NIH/3T3 cells transfected in stable Kat2b KO and control cells. After serum-free treatment, cells were fixed and stained using ICC in a time-course manner. Acetylated α-tubulin was stained for primary cilia (green). Nuclei were stained with DAPI (blue). Primary cilia are indicated by white arrows. Scale bar: 10 μm. (**h**) Quantification of the percentage of ciliated cells in Kat2b-depleted cells compared to control shRNA cells. Counted cell numbers were as follows: controls with serum starvation for 6 h, n = 685; 12 h, n = 665; 24 h, n = 589. Kat2b-depleted cells with serum starvation for 6 h, n = 789; 12 h, n = 579; 24 h, n = 649. Data were collected from three independent experiments.

serum starvation. Time-course analysis revealed that the mRNA levels (Fig. 1a) and protein (Fig. 1b) of Kat2b gradually increased. These data indicated that Kat2b plays a specific role in ciliogenesis. Although Kat2b has been recognized to predominantly localize to the nucleus, a recent study found that Kat2b also localizes to the centrosome[25]. However, Kat2b localization to primary cilia has yet to be characterized. Thus, the subcellular localization of Kat2b during primary cilia biogenesis was examined to verify whether Kat2b is associated with primary cilia as a transcriptional coactivator in the nucleus or in other cellular locations. NIH/3T3 cells were transfected with expression vectors containing DsRed-tagged Kat2b. The next day, cells were serum-starved and fixed at 0 h, 6 h, 12 h and 24 h. Confocal microscopy revealed the subcellular localization of Kat2b (Fig. 1c,d). Initially, 83.2% of Kat2b was localized mainly in the nucleus, and only approximately 16.8% of Kat2b existed in the cytosol and centrosome. Interestingly, the proportion of Kat2b localized in the cytosol and centrosomes slightly increased 6 h after serum starvation. Moreover, the proportion increased by approximately 2.5 times as ciliogenesis progressed. Interestingly, Kat2b was also found to localize to the basal body. These findings demonstrate that Kat2b localizes to the cytosol, centrosomes, and basal body during ciliogenesis, suggesting that it plays a potential role in primary cilia formation.

Loss of Kat2b delays ciliogenesis

To evaluate the role in ciliogenesis in vitro, Kat2b-depleted NIH/3T3 cells were generated using short hairpin RNA (shRNA) against Kat2b. The cells were then incubated under serum-starved conditions. The cells were then harvested or fixed in a time-dependent manner. Kat2b expression was found to decrease by qRT-PCR and western blotting compared to the control group (Fig. 1e,f). Using immunocytochemistry, the number of primary cilia assembled at each time point was determined. The ablation of Kat2b proteins led to a decreased percentage of ciliated cells at 6 and 12 h after serum starvation, indicating that Kat2b depletion causes retention of ciliogenesis at an early stage (Fig. 1g,h). In contrast, there was no significant difference in the percentage of ciliated cells at 24 h starvation, and it implied that loss of Kat2b has less effect on primary cilia overall maturation. Thus, the results indicate that Kat2b is required for the appropriate initiation of ciliary formation.

Kat2b regulates the acetylation of α-tubulin via its acetyltransferase function

Acetylated microtubules, such as the axoneme of primary cilia, are considered long-lived[17]. According to a previous study, the acetylation of α-tubulin increases the flexibility of microtubules, contributing to better resistance against mechanical stress and consequently making them long-lived[26]. Acetylated-α-tubulin on lysine 40 residue is a cilia marker. Thus, the data led us to investigate the possibility that Kat2b regulates primary cilia through the acetylation of α-tubulin as a non-histone target of Kat2b (Fig. 2a).

First, whether Kat2b affects the level of acetylated tubulin was evaluated. The western blot data showed that although Kat2b depletion impaired the level of acetylated α-tubulin both early and late serum starvation, the total amount of α-tubulin did not change (Fig. 2b). To verify whether the regulation of acetylated α-tubulin would be dependent on the existence of Kat2b, an over-expressed Kat2b flag-tagged plasmid (FL-Kat2b) was transferred into Kat2b-depleted cells with 6 h and 24 h serum starvation. The data revealed that acetylated α-tubulin levels were rescued in Kat2b-depleted cells when FL-Kat2b was transfected, while the transfection itself did not affect the acetylation level of α-tubulin (Fig. 2c). Based on these results, whether Kat2b regulates the acetylation level of α-tubulin by interacting with it was evaluated. The immunoprecipitation results revealed that both Kat2b and α-tubulin existed in the cell lysate and that Kat2b interacted with α-tubulin endogenously (Fig. 2d). In addition, α-tubulin interacted with Kat2b and vice versa. To validate disrupted cilia assembly by Kat2b absence, comparison between Arl13b, well-established ciliary marker, and acetylated α-tubulin was verified (Fig. 2e,f). Both serum withdrawal 6 h and 24 h under silence Kat2b had no significant difference between Arl13b and acetylated α-tubulin, but the intensity of acetylated α-tubulin itself and Arl13b were reduced.

According to previous research, garcinol inhibits the acetyltransferase activity of Kat2b[27]. In addition, cytoplasmic acetylated lysine decreases in garcinol-treated human U2OS cells[28]. Thus, NIH/3T3 cells were treated with 500 nM garcinol and serum starved them for 6 h to induce the early stage of ciliogenesis, which was delayed by Kat2b depletion. The results indicated that the percentage of ciliated cells in the DMSO-treated group was approximately 25%, whereas the percentage significantly decreased in garcinol-treated cells, showing that approximately 12% of the cells were ciliated (Fig. 2g,h). In addition, the acetylated α-tubulin level normalized Kat2b was also decreased in the garcinol-treated group compared to that in the control group (Fig. 2h). More importantly, garcinol disrupted Kat2b localization within primary cilia, particularly in basal body (Fig. 2i). Taken together, these findings highlighted the novel result that α-tubulin is a non-histone target of Kat2b. Kat2b was revealed to interact with α-tubulin endogenously and regulate its acetylation level in a Kat2b-dependent manner. Moreover, these findings demonstrated that Kat2b hampers the cilium assembly rate and acetylation of α-tubulin via its acetyltransferase function.

Kat2b is required for the recruitment of IFT proteins and the Hedgehog signaling pathway component to the primary cilia

Microtubules, which have α-tubulin as their subunit, act as a highway for many molecules, including IFT particles[29]. Previous studies have revealed that microtubule stability is regulated by acetylation[30]. The fact that Kat2b functions in the acetylation of α-tubulin suggests that the weakened microtubule could not break the highway but could hamper cargo transport along the microtubule. Thus, whether the IFT components may be affected by Kat2b depletion was evaluated herein.

In the early stages of primary cilia assembly, the western blotting data showed that IFT25, IFT46, IFT52, and IFT140, which are involved in cilia assembly, decreased in the whole lysate of NIH/3T3 cells when Kat2b was silenced (Fig. 3a and Supplementary Fig. 1a). To exclude the possibility that Kat2b regulates the levels of IFT components through its histone acetyltransferase function, the mRNA levels of IFT components in whole lysates
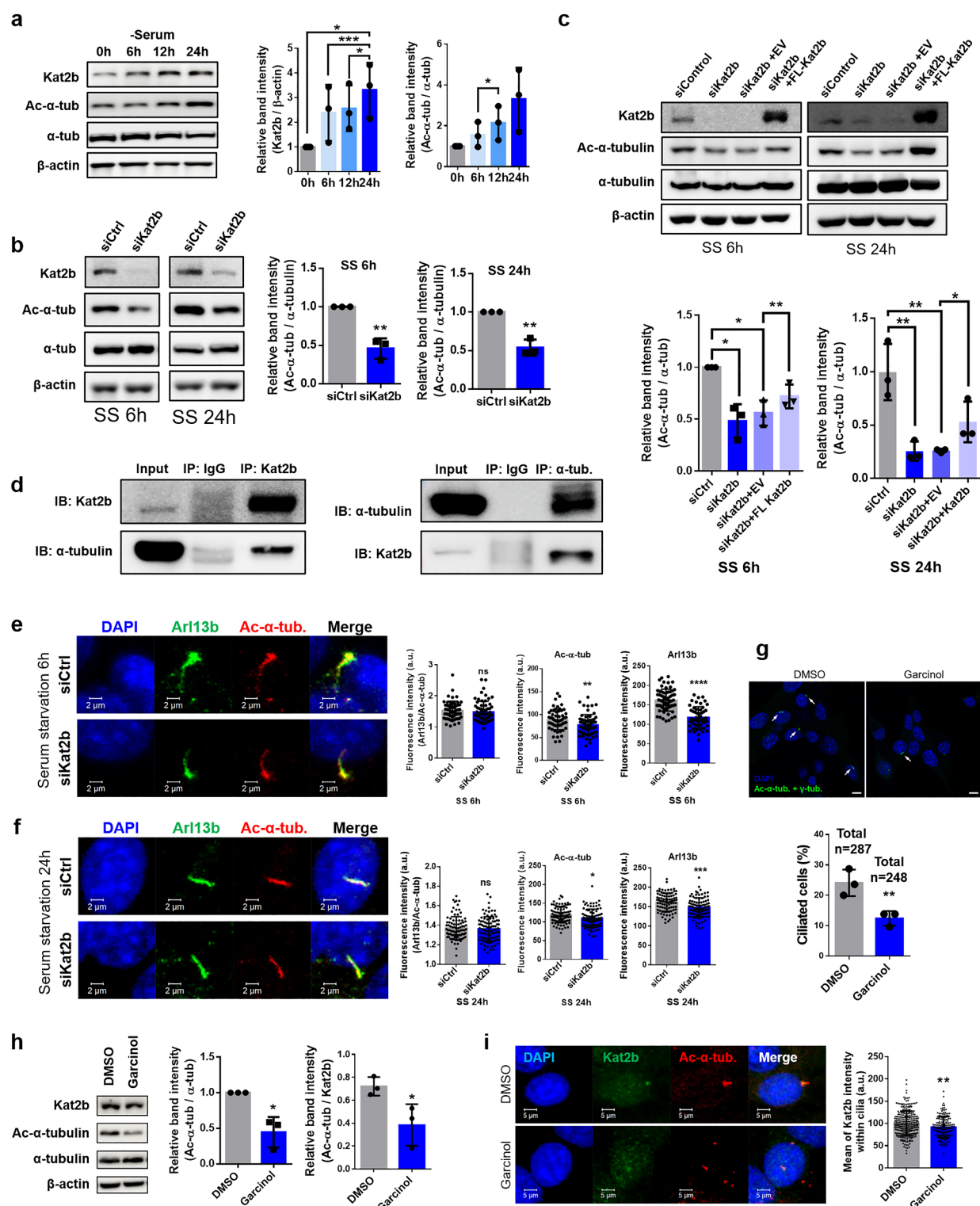
of NIH/3T3 cells after 6 h of serum starvation were determined. Interestingly, the transcript levels of some IFTs were either slightly increased or unchanged in Kat2b-depleted cells (Supplementary Fig. 1c).

Based on these findings, immunocytochemistry experiments were conducted to verify whether the loss of Kat2b affected the ciliary-localized IFT components. Stable Kat2b knockdown cells were used to verify the localization of IFT components with or without Kat2b expression (Fig. 3b). The confocal microscopy data revealed that IFT25 was localized to the basal body and IFT52 was stained at the basal body, axoneme, and ciliary tip in shControl NIH/3T3 cells at an early stage of ciliogenesis. Interestingly, the fluorescence intensities of IFT25 and IFT52 were decreased in stable Kat2b knockdown cells (Fig. 3e). However, the intensities of IFT46 and IFT140 were not changed in Kat2b-depleted cells (Supplementary Fig. 2a,b).

Unexpectedly, the western blotting results indicated that the majority of IFT components decreased after 24 h of serum starvation, which is at the maturation stage of ciliogenesis, whereas the mRNA levels either increased

Fig. 2. Kat2b interacts with and regulates the acetylation level of α-tubulin. (**a**) Western blots showing Kat2b and acetylated α-tubulin expression at 0, 6, 12, and 24 h after serum withdrawal. The graphs showed relative western blotting band intensity of Kat2b and acetylated-α-tubulin normalized each loading controls. Data were collected from three independent experiments. Statistical analysis for normalizing band was conducted by paired t-test. (**b**) Acetylated α-tubulin expression was decreased in Kat2b silenced NIH/3T3 cells at 6 h and 24 h after serum starvation. The graphs next to immunoblot analysis showed quantified acetylated α-tubulin band intensity. (**c**) Western blot data showed that overexpression of Kat2b restored the decreased acetylation level of α-tubulin in Kat2b silenced cells at 6 h and 24 h after serum starvation. The relative band intensity of α-tubulin acetylation was displayed through the graphs below. EV indicates empty vector (pCMV-tag2B) and FL-Kat2b indicates full length Kat2b-pCMV-tag2B. (**d**) Immunoprecipitation data revealed that endogenous Kat2b interacts with α-tubulin in NIH/3T3 cells. (**e, f**) Fluorescence images showed comparison between ciliary markers under Kat2b silencing with serum starvation 6 h, 24 h. Arl13b marked ciliary membrane (green), ac-α-tubulin, marked ciliary axoneme (red), and nuclei were stained with DAPI (blue). Graphs on right side indicated fluorescence intensity of Arl13b normalized ac-α-tubulin, ac-α-tubulin and Arl13b, respectively. This experiments were independently repeated in triplicate and graphs were analyzed by two-tailed Student's t-test and values are presented as the mean ± SD. (**g**) Fluorescence images represented ciliated cells with or without 500 nM garcinol treatment for 6 h with serum starvation. Acetylated α-tubulin and γ-tubulin were stained for primary cilia (green). Nuclei were stained with DAPI (blue). Primary cilia are indicated by white arrows. White arrows indicate primary cilia. Scale bar: 10 μm. The graph showed quantification of the percentage of primary cilia in garcinol-treated cells compared to DMSO-treated NIH/3T3 cells. Counted cell numbers were as follows: DMSO-treated cells n = 287, garcinol-treated cells n = 248. (**h**) Western blot data showed that the acetylation level of α-tubulin decreased in garcinol-treated NIH/3T3 cells. Graphs on right side showed relative western blotting band intensity of acetylated-α-tubulin normalized α-tubulin and acetylated-α-tubulin normalized Kat2b. (**i**) Images represented localization of Kat2b within cilia when treated garcinol, and graph displayed mean of Kat2b fluorescence intensity within acetylated-α-tubulin. Data collected from three experiments were quantified graphically.

slightly or remained unchanged (Fig. 3c and Supplementary Fig. 1b and d). At this later stage, IFT25 was strongly stained in the basal body and IFT52 was also localized in the basal body and axoneme (Fig. 3d). Surprisingly, the immunocytochemistry data clearly showed that the intensity of IFT fluorescence markedly decreased in shKat2b cells (Fig. 3e). This is unexpected because the depletion of Kat2b did not show a decreased percentage of ciliated cells at the time point of 24 h after serum starvation. The results imply that even though cilia formation was saturated in Kat2b-depleted cells to the same extent as in the control cells, ciliary function may be damaged. To confirm these results, whole-body Kat2b knockout mouse embryonic fibroblast (MEF) cell lines were used. Intriguingly, the fluorescence intensities of IFT25 and IFT52 were found to be significantly reduced in Kat2b knockout (KO) MEF cells at 6 h and 24 h of serum starvation (Fig. 3f,g). Additionally, acetyl transferase inactivation of Kat2b using garcinol was confirmed to attenuate ciliary recruitment of IFT52 (Fig. 3h). These results suggest that the function of Kat2b in regulating acetylation of α-tubulin influences the ciliary recruitment of some IFT proteins.

Since the loss of IFT25 impairs Hedgehog (Hh) signaling[31] and the depletion of Kat2b hampers Hh signaling in a cancer model[32], whether the ablation of Kat2b expression could affect the activation of Hh signaling in the context of primary cilia was evaluated. To test this, Kat2b were silenced and exposed to serum starvation with 500 nM SAG (Smo agonist) the following day for 24 h. SAG (Smo agonist), an activator of Hh signaling, binds to the heptahelical bundle of the Smo protein[33] and induces ciliary translocation of Smo, leading to the activation of Hh signaling. The data showed that Smo was recruited to the primary cilia, despite the lack of SAG treatment in Kat2b depleted cells (Fig. 4a). Upon treatment with SAG, Smo was recruited to the whole axoneme with strong fluorescence intensity in control NIH/3T3 cells, whereas the fluorescence intensity of the Smo protein was significantly decreased in Kat2b depleted cells (Fig. 4a). Next, both the mRNA and protein levels of Gli1, an Hh signaling marker, were found to increase in SAG-treated cells, but not as much as when Kat2b was depleted (Fig. 4b,c). The recruitment of Smo protein at the primary cilia and Gli1 mRNA levels were also impaired in Kat2b knockout MEF cells (Fig. 4d,e). Furthermore, when cells treated SAG with serum starvation 24 h after garcinol treatment for 6 h, fluorescence intensity of Smo reduced as well (Fig. 4f). Taken together, these findings indicate that IFT recruitment and Hh signaling in primary cilia are damaged when Kat2b is absent.

Function of acetyltransferase Kat2b for ciliogenesis depends upon the localization in cytosol

To investigate the α-tubulin acetylation function of Kat2b in detail, an acetyltransferase domain-deleted construct of Kat2b (ΔAT), a nuclear localization signal domain-deleted Kat2b (ΔNLS) and both-domain-deleted Kat2b mutant (ΔATΔNLS) were created (Fig. 5a). Through immunocytochemistry experiments, it was confirmed that DsRed tagged ΔNLS-Kat2b and ΔATΔNLS-Kat2b were not located in nucleus (Fig. 5b). The non-nuclear localization of GFP-tagged-ΔNLS-Kat2b and ΔATΔNLS-Kat2b was also identified but GFP-tagged-FL-Kat2b existed in nucleus by separation of nuclear and cytoplasmic fraction experiments (Fig. 5c). NIH/3T3 cells were transfected with the GFP-tagged Kat2b construct for 48 h, and the harvested cells were immediately separated into cytosolic and nuclear fractions. The immunoblotting band intensities were normalized with each loading control: α-tubulin as a cytosol control and histone H3 as a nuclear control. The percentage of Kat2b found in the nucleus versus the cytoplasm was graphically represented. Less than half of the NLS domain-depleted Kat2b were localized in the nucleus, and the NLS and AT domain-depleted Kat2b were in a nearly nonnuclear position. The tagged vector was replaced with GFP to avoid overlap with the fluorescence wavelength that identifies the
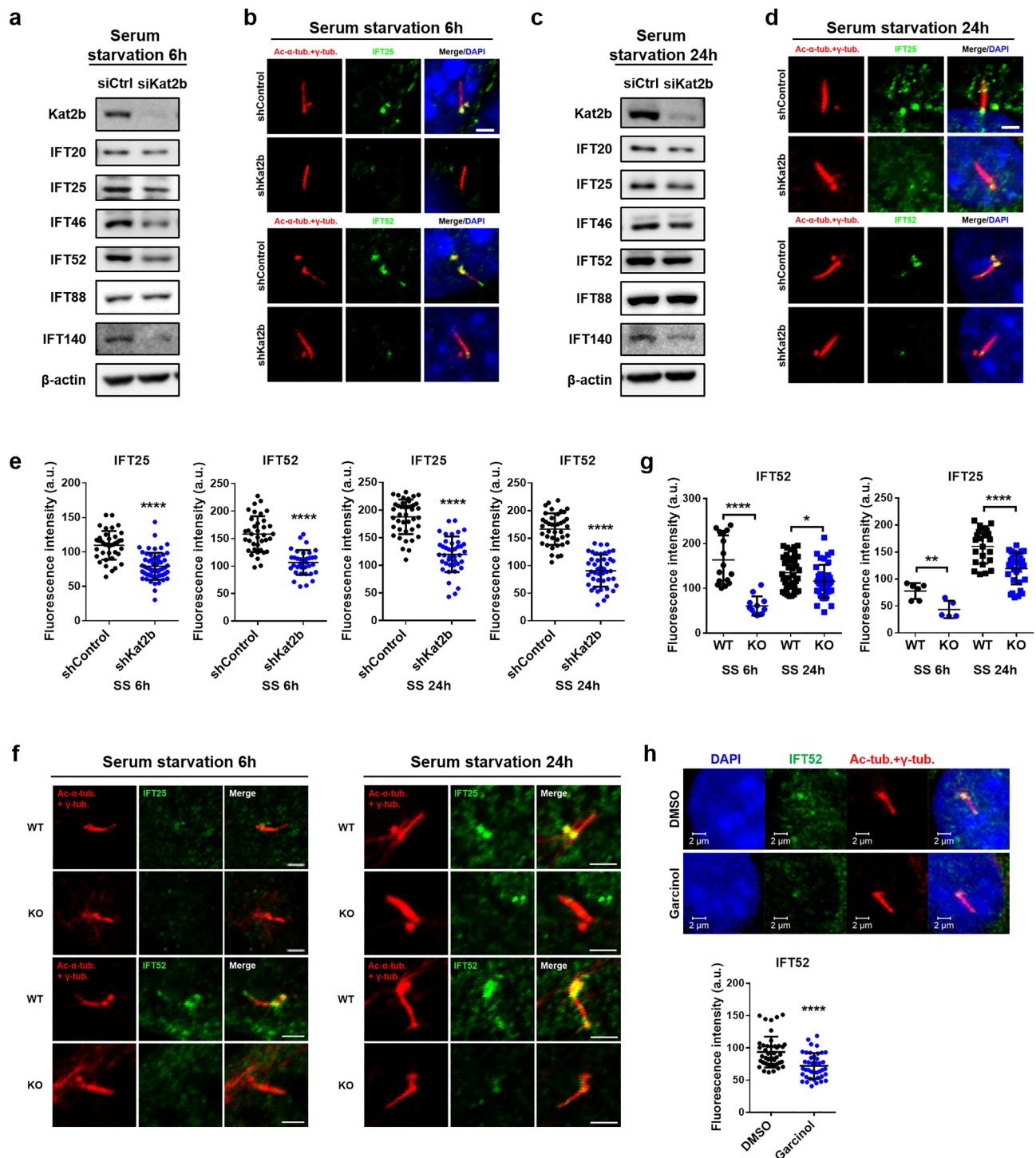
Fig. 3. The depletion of Kat2b impairs the recruitment of IFT and Hh components to primary cilia. (**a, b**) IFT components 6 h after serum starvation (early ciliogenesis). (**a**) Western blot data showed that protein levels of IFT components decreased in Kat2b silenced NIH/3T3 cells. (**b**) Fluorescence staining data revealed that the intensity of IFT components located in primary cilia was decreased in the stable Kat2b deleted cell. Scale bar: 2 μm (**c-d**) IFT components 24 h after serum starvation (maturated stage of ciliogenesis). (**c**) Western blot data show that protein levels of IFT components decreased in Kat2b silenced NIH/3T3 cells. (**d**) Immunocytochemistry data revealed that fluorescence intensity of IFT components located in primary cilia. Scale bar: 2 μm (**e**) Graphs showed fluorescence intensity of IFT25 and IFT52 under serum starvation 6 h, 24 h in stable Kat2b KO NIH3Te and control NIH3T3. (**f**) Immunocytochemistry data display that the fluorescence intensity of IFT25 and IFT52 (green) at primary cilia (red) in Kat2b KO MEF cells at 6 h and 24 h after serum starvation, respectively. Scale bar: 2 μm. (**g**) Graphs showed fluorescence intensity of IFT25 and IFT52 under serum starvation 6 h, 24 h in MEF cells. (**h**) Representative images displayed accumulation of IFT52 within cilia when treated garcinol and serum withdrawal 6 h, and below graph showed fluorescence intensity at cilia.
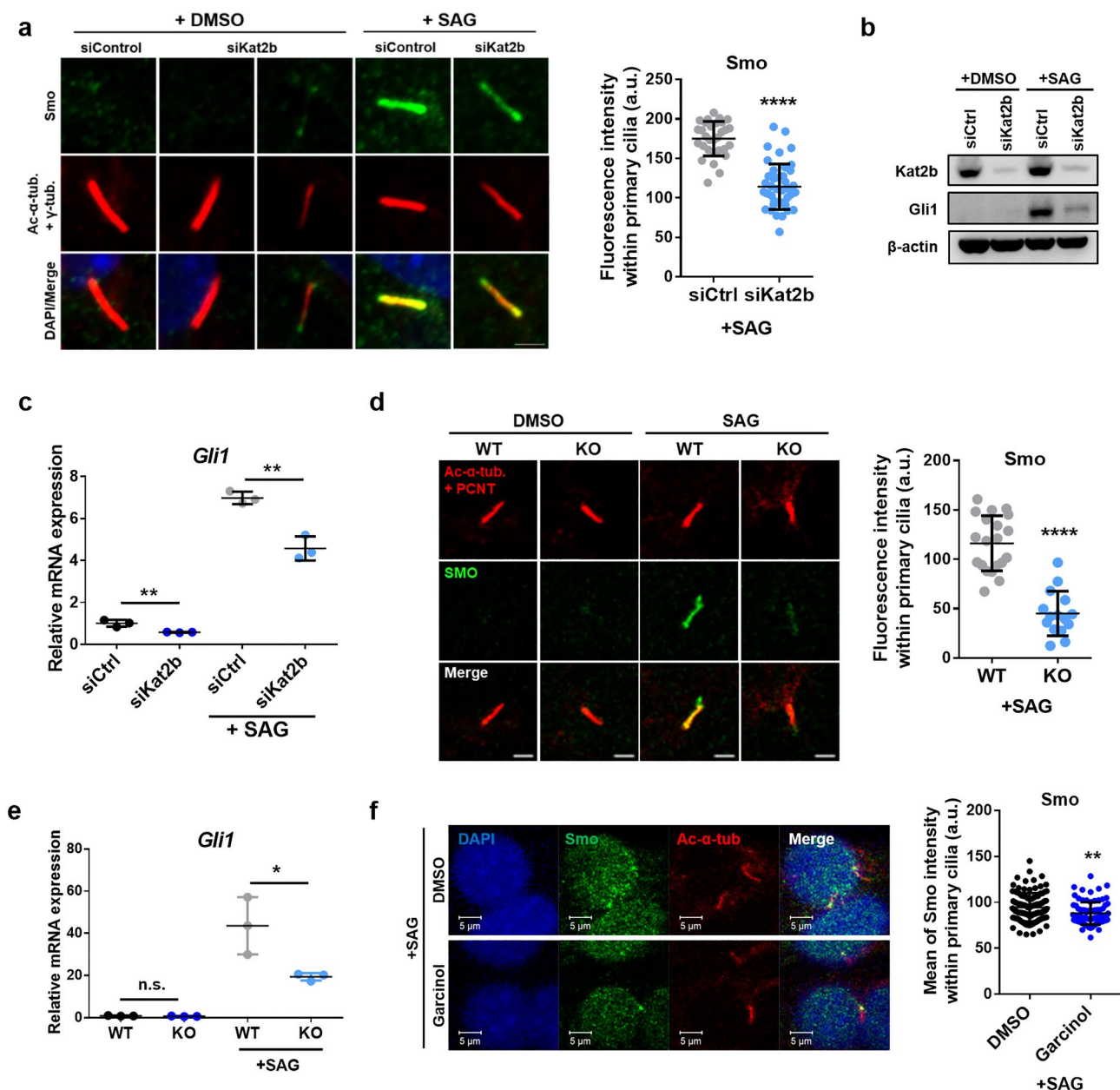
Fig. 4. Kat2b knockdown impairs the recruitment of Hh components to primary cilia. (**a**) Immunocytochemistry data confirmed that the fluorescence intensity of Smo (green) was decreased in Kat2b silenced cell. Acetylated α-tubulin and γ-tubulin were stained for primary cilia and basal body (red). Nuclei were stained with DAPI (blue). Scale bar: 2 μm Right graph showed fluorescence intensity of Smo within primary cilia. (**b**, **c**) qRT-PCR and western data showed that mRNA and protein levels of Gli1 expression were decreased when Kat2b was depleted by siRNA transfection. Gli1 was used as an activation marker of the Hh signaling pathway. NIH/3T3 cells were treated with serum starvation for 24 h and 500 nM of SAG for activation of Hh signaling. (**d**) Immunocytochemistry data of Smo protein (green) at primary cilia (red) in Kat2b KO MEF cells with serum starvation for 24 h and 400 nM of SAG. Scale bar: 2 μm. Right graph showed fluorescence intensity of Smo within primary cilia. (**e**) qRT-PCR data showing that transcriptional Gli1 expression was decreased in Kat2b KO MEF cells. (**f**) Representative images displayed accumulation of Smo within primary cilia when treated garcinol 6 h before SAG treatment and serum withdrawal 24 h, and right graph showed mean of fluorescence intensity within cilia.

IFT52 and proceeded with the following experiment. As observed in Fig. 3d, the ciliary localization of IFT52 in shControl NIH/3T3 cells with the empty vector was situated at the cilia, and less ciliary distribution was observed in shKat2b NIH/3T3 cells with the empty vector (Fig. 5d). In full-length-Kat2b transfected shKat2b NIH/3T3 cells that had undergone complete recovery, the localization proportion of IFT52 with cilia surpassed that of shControl cells, and almost all IFT52 was found in the ciliary structure of transfected cells. ΔAT and
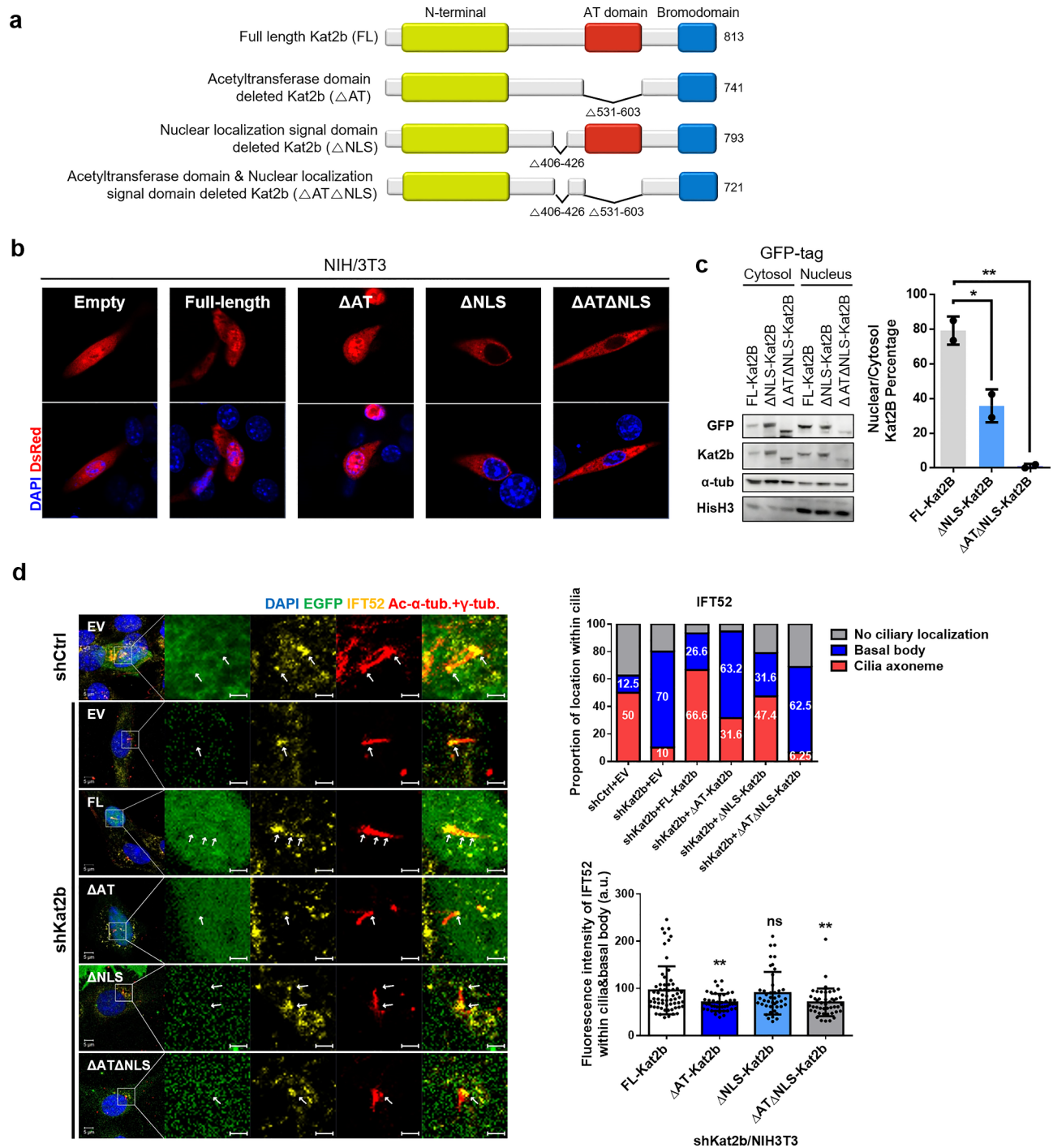
Fig. 5. The acetyltransferase domain of Kat2b in the cytosol is significant for localization of IFT components at primary cilia. (**a**) Graphical view of domains of Kat2b and designed mutant Kat2b. (**b**) Immunocytochemistry images confirmed the localization of the designed mutant Kat2b construct. DsRed tagged Kat2b constructs were investigated vector transfected cell and nuclear localization signal domain deleted Kat2b positioned only cytosol. (**c**) Immunoblotting analysis verified cytosolic and nucleic distribution under transfection with Kat2b constructs in NIH/3T3 cell. α-tubulin represented as cytosol marker and histone H3 as nuclear marker. (**d**) Immunofluorescence images showed that IFT 52 localization depending on Kat2b existence in the nucleus and function of acetylation. shControl NIH/3T3 cells transfected by empty vector, and stable Kat2b depleted NIH/3T3 cells, as shKat2b, transfected by empty vector and mutant Kat2b constructs. Nuclei were stained with DAPI (blue), transfected vector constructs were EGFP (green), acetylated α-tubulin and γ-tubulin were stained for primary cilia (red), and IFT52 were indicated yellow. White arrows indicate IFT components located in the cilia axoneme. The proportion of IFT52 distribution by categories are displayed below the graphs; ciliary axoneme, basal body, and not on the cilia. The graph on the bottom right indicated fluorescence intensity of ciliary IFT52. Scale bar: 2 μm.

ΔATΔNLS constructs were transfected into stable Kat2b-depleted cells, as expected, proportion of IFT52-positive cilia decreased compared to that in FL-Kat2b transfected cells at maturation stages of primary cilia assembly. ΔATΔNLS -Kat2b in Kat2b-depleted cells in particular was acted as an empty vector, since the ratio of IFT52 on the cilia and basal bodies was extremely similar. Finally, in ΔNLS-Kat2b-transfected shKat2b cells, a nearly complete recovery was observed with ciliary localization of IFT52, analogous to the shControl cells. These results indicate that the function of Kat2b as an acetyltransferase was significant for the correct localization of IFT52. Thus, cytoplasmic Kat2b alone may play a sufficient role in the localization of IFT components in the cilia.

Kat2b knockout mice show mild abnormalities related to cilia defects in kidneys

To test whether Kat2b depletion in vivo closely reflected the in vitro results, the kidney tissue of a Kat2b knockout (KO) mouse model was examined. Primary cilia are found in the apical region of renal epithelial cells[34], and previous studies have revealed that IFT defects cause ciliopathies, such as cystic kidney disease[35,36]. Because no significant developmental phenotype was found in kat2b KO in published papers[23], there is still a lack of research on disease phenotypes caused by Kat2b defects. First, the level of Kat2b was found to decrease in Kat2b KO mice (Fig. 6a and b). Although the value of two kidney weights per total body weight did not change (Fig. 6c), Kat2b KO mice showed decreased expression of acetylated alpha tubulin (Fig. 6d). Hematoxylin and eosin staining revealed that Kat2b KO mice have mild abnormalities in the kidneys. They showed dilated tubules and loosened glomeruli, whereas the wild-type kidneys showed tight glomeruli (Fig. 6e). This is interesting because disruption of the primary cilia component causes glomerular cysts[37,38]. Since the in vitro data (Fig. 3) revealed that the loss of Kat2b impairs the recruitment of IFT components to primary cilia, immunofluorescence experiments were conducted to investigate whether IFT defects also exist in vivo. Confocal microscopy showed that the fluorescence intensity of IFT25 in primary cilia decreased in Kat2b KO, whereas IFT25 was distributed over the cilia of renal tubules in WT mice (Fig. 6f). These results indicate that the loss of Kat2b caused primary ciliary defects in vivo.

Discussion

In this study, Kat2b was investigated as a potential novel regulator of primary cilia using in vitro and in vivo experiments. The results suggest that the loss of Kat2b caused a delay in ciliogenesis and reduced the acetylation of α-tubulin through its acetyltransferase activity. Importantly, Kat2b depletion hampered the recruitment of IFT components to the cilium and decreased Hh signaling activation. Eventually, Kat2b KO mice showed mild renal abnormalities and aberrant IFT25 recruitment. These findings strongly imply a relationship between Kat2b and the acetylation of α-tubulin, which organizes primary cilia. In the early stages of primary cilia assembly, loss of Kat2b disrupts α-tubulin acetylation. As a result, IFT25 and IFT52 were found to be abnormally positioned. Despite Kat2b defects, the structural maturation of primary cilia was possible; however, the expression and accumulation of some IFTs and Smo within primary cilia appeared abnormal. (Fig. 7).

These results are supported by two recently published papers on the relationship between primary cilia and other PTMs, such as polyglutamylation. The authors suggested that polyglutamylation itself does not impair the primary cilia phenotype; however, it regulates the function of primary cilia via the Hh signaling pathway[39,40]. This supports our hypothesis and results, considering that cilium assembly was compensated for at the late stage of ciliogenesis in Kat2b depleted cells, although Kat2b regulates ciliary functions such as IFTs and the Hh signaling pathway. This suggests that PTMs in the primary cilium, such as acetylation and polyglutamylation, are involved in the functional aspects of primary cilia rather than assembly and have shared roles.

A recent proteomic approach conducted by Fournier et al. to identify the Kat2b-targeted acetylome[25] may provide insights into this. For example, KIF17 may be targets of Kat2b. KIF17 is a member of the kinesin-2 family and contributes to IFT-B transport[41,42]. More interestingly, their acetylome data uncovered many proteins related not only to motor proteins but also to other primary ciliary proteins that could be acetylated by Kat2b; for instance, ALMS1 is an Alstrom syndrome gene, which is ciliopathic[43]. DZIP1L is another ciliopathic gene that encodes the ciliary transition zone protein and is associated with autosomal recessive polycystic kidney disease (ARPKD)[44]. SDCCAG3 has also been reported to localize to the basal body and interact with IFT88[45]. TTBK2 is a ciliary gene that is involved in the early stages of ciliogenesis[46]. These results provide strong evidence for the ciliary role of Kat2b. Further investigation is needed to elucidate the possible relationship between Kat2b and other primary ciliary proteins.

Combined with previous studies, the findings presented in this study provide evidence for the development of therapeutic approaches for ciliopathies. The results revealed that Kat2b regulates primary ciliary function. Furthermore, Kat2b KO mice were found to show mild pathological effects, including glomerular abnormalities and dilated tubules in the kidney. Whether Kat2b upregulation attenuates this pathological effect and recover ciliary function requires further investigation. Taken together, these findings highlight the novel role of Kat2b in regulating primary cilium function and its pathological effects on the kidney.
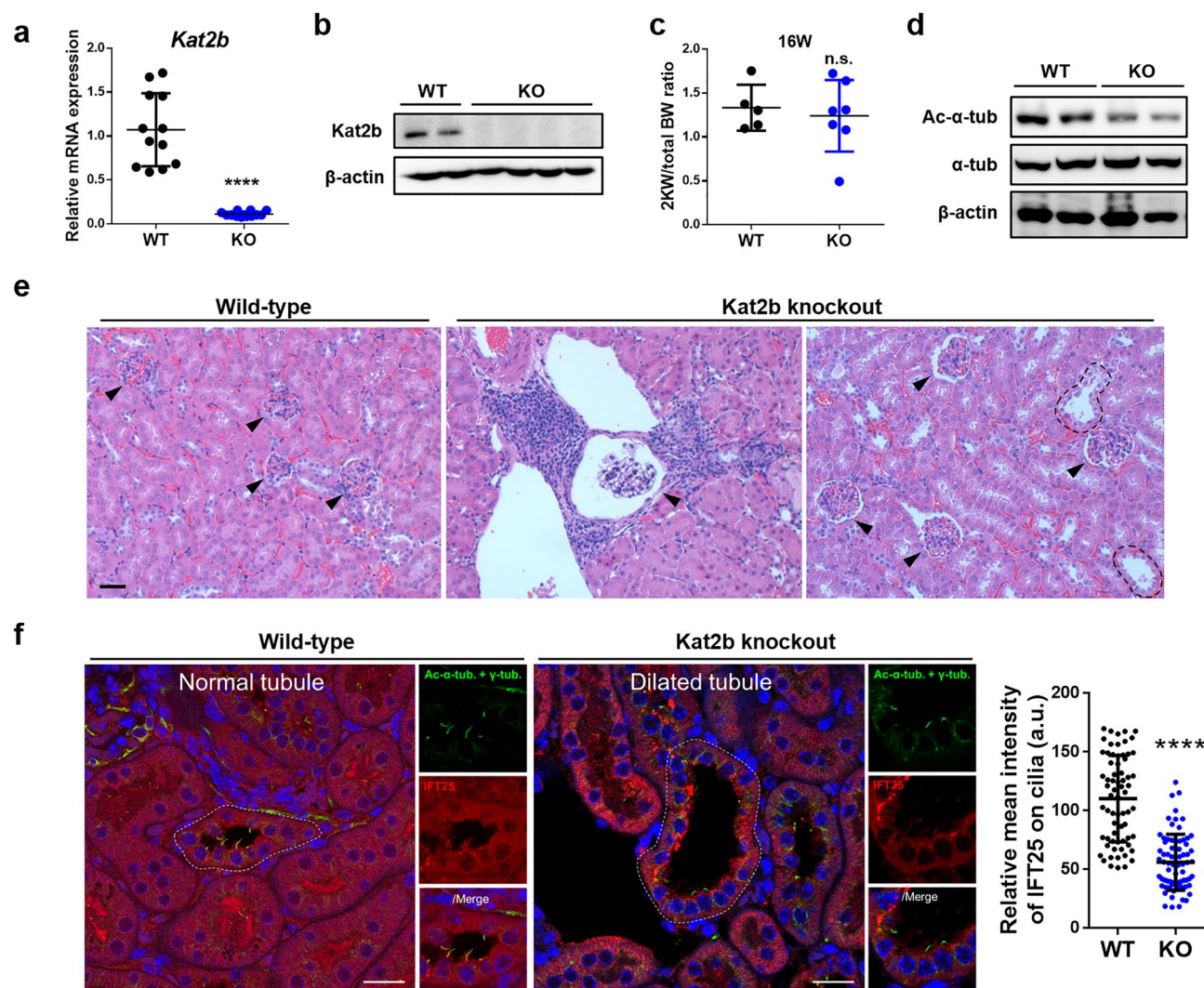
Fig. 6. Kat2b knockout mice show decreased IFT25 in primary cilia and renal abnormalities. (**a**) Kat2b mRNA expression data using qRT-PCR validated that the level of Kat2b was decreased in the kidney of Kat2b KO mice. (**b**) Western blots also showed decreased Kat2b expression in KO mice. (**c**) Two kidney weights per total body weight demonstrate that there were no significant differences between Kat2b KO mice and wild-type mice. (**d**) Western blot data showed that acetylated α-tubulin level decreased in the renal tissue of Kat2b KO mice. (**e**) H&E staining of kidney paraffin sections from 16 weeks Kat2b knockout mice showed glomerular cyst, loosen glomeruli, and dilated tubules. Black arrowheads indicate glomeruli. The black dotted line defines the area of the dilated tubule. Scale bar: 100 μm. (**f**) Confocal microscopy analysis revealed that the fluorescence intensity of IFT25 (red) at primary cilia decreased in the renal tubule from 16 weeks Kat2b knockout mice compared to the wild-type. Acetylated α-tubulin and γ-tubulin were stained for primary cilia (green). Nuclei were stained with DAPI (blue). The White dotted line defines the area of the renal tubule. Right graph showed relative mean of IFT25 fluorescence intensity within primary cilia. Scale bar: 20 μm.
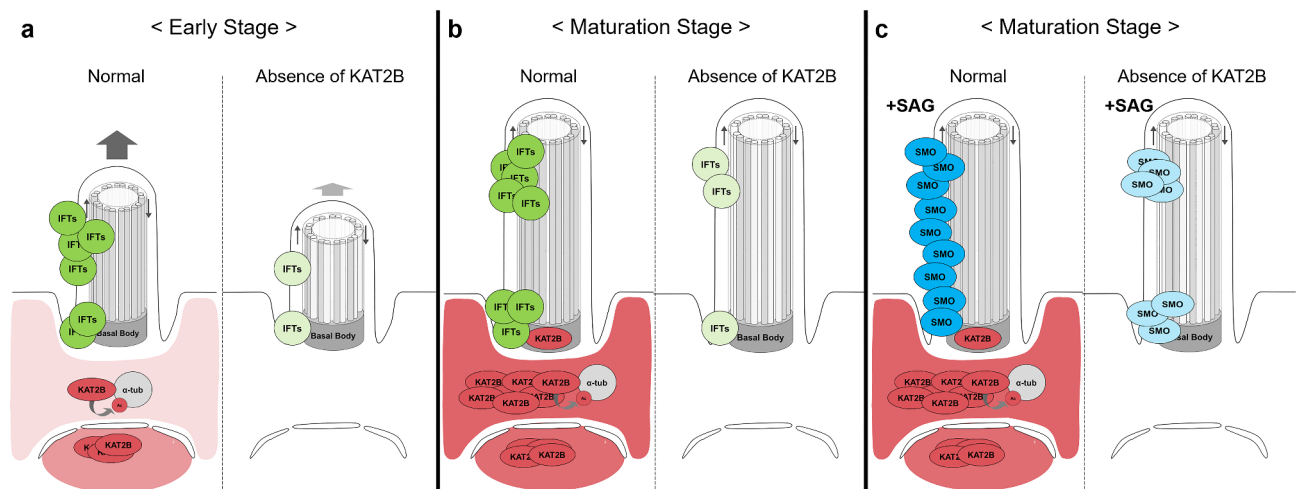
Fig. 7. Summary illustration of this study. Red ovals indicate KAT2B; green circles indicate IFT-B particles; blue circles indicate SMO; light grey circles indicate α-tubulin. The color intensity indicates the abundance. (**a**, **b**) During ciliogenesis, the basal expression level and subcellular localization of Kat2b in the cytosol, centrosome, and basal body gradually increased. Kat2b interacts with α-tubulin and regulates the acetylation level of α-tubulin via its catalytic activity. When Kat2b was depleted, the rate of cilium assembly was delayed, causing less acetylation level of α-tubulin, and the recruitment of IFT to be impaired. (**c**) When the Hh signaling pathway was activated using SAG treatment, the recruitment of SMO along the cilium is less under the absence of Kat2b.

Data availability
All data generated and/or analyzed during this study are available from the corresponding author upon reasonable request.

References
1. Satir, P., Pedersen, L. B. & Christensen, S. T. The primary cilium at a glance. *J. Cell Sci.* **123**, 499–503. https://doi.org/10.1242/jcs.050377 (2010).
2. Bloodgood, R. A. From central to rudimentary to primary: the history of an underappreciated organelle whose time has come. The primary cilium. *Methods Cell Biol.* **94**, 3–52. https://doi.org/10.1016/S0091-679X(08)94001-2 (2009).
3. Barr, M. M. & Sternberg, P. W. A polycystic kidney-disease gene homologue required for male mating behaviour in *C. elegans*. *Nature* **401**, 386–389. https://doi.org/10.1038/43913 (1999).
4. Fliegauf, M., Benzing, T. & Omran, H. When cilia go bad: cilia defects and ciliopathies. *Nat. Rev. Mol. Cell Biol.* **8**, 880–893. https://doi.org/10.1038/nrm2278 (2007).
5. Kim, J. B. et al. Increased ER stress by depletion of PDIA6 impairs primary ciliogenesis and enhances sensitivity to ferroptosis in kidney cells. *BMB Rep.* **57**, 453–458. https://doi.org/10.5483/BMBRep.2023-0247 (2024).
6. Han, Y. G. et al. Dual and opposing roles of primary cilia in medulloblastoma development. *Nat. Med.* **15**, 1062–1065. https://doi.org/10.1038/nm.2020 (2009).
7. Munoz-Estrada, J., Lora-Castellanos, A., Meza, I., Alarcon Elizalde, S. & Benitez-King, G. Primary cilia formation is diminished in schizophrenia and bipolar disorder: A possible marker for these psychiatric diseases. *Schizophr. Res.* **195**, 412–420. https://doi.org/10.1016/j.schres.2017.08.055 (2018).
8. Huangfu, D. & Anderson, K. V. Cilia and Hedgehog responsiveness in the mouse. *Proc. Natl. Acad. Sci. U.S.A.* **102**, 11325–11330. https://doi.org/10.1073/pnas.0505328102 (2005).
9. Singla, V. & Reiter, J. F. The primary cilium as the cell's antenna: signaling at a sensory organelle. *Science* **313**, 629–633. https://doi.org/10.1126/science.1124534 (2006).
10. Gluenz, E. et al. Beyond 9+0: Noncanonical axoneme structures characterize sensory cilia from protists to humans. *FASEB J. Off. Publ. Fed. Am. Soc. Exp. Biol.* **24**, 3117–3121. https://doi.org/10.1096/fj.09-151381 (2010).
11. Ainsworth, C. Cilia: tails of the unexpected. *Nature* **448**, 638–641. https://doi.org/10.1038/448638a (2007).
12. Rosenbaum, J. L. & Witman, G. B. Intraflagellar transport. *Nat. rev. Mol. cell Biol.* **3**, 813–825. https://doi.org/10.1038/nrm952 (2002).
13. Hsiao, Y. C., Tuz, K. & Ferland, R. J. Trafficking in and to the primary cilium. *Cilia* **1**, 4. https://doi.org/10.1186/2046-2530-1-4 (2012).
14. Janke, C. The tubulin code: Molecular components, readout mechanisms, and functions. *J. Biol.* **206**, 461–472. https://doi.org/10.1083/jcb.201406055 (2014).
15. Magiera, M. M. & Janke, C. Post-translational modifications of tubulin. *Curr. Biol. CB* **24**, R351-354. https://doi.org/10.1016/j.cub.2014.03.032 (2014).
16. You, E. et al. Casein kinase 2 promotes the TGF-beta-induced activation of alpha-tubulin acetyltransferase 1 in fibroblasts cultured on a soft matrix. *BMB Rep.* **55**, 192–197 (2022).
17. Janke, C. & Montagnac, G. Causes and consequences of microtubule acetylation. *Curr. Biol. CB* **27**, R1287–R1292. https://doi.org/10.1016/j.cub.2017.10.044 (2017).

18. Shida, T., Cueva, J. G., Xu, Z., Goodman, M. B. & Nachury, M. V. The major alpha-tubulin K40 acetyltransferase alphaTAT1 promotes rapid ciliogenesis and efficient mechanosensation. *Proc. Natl. Acad. Sci. U. S. A.* **107**, 21517–21522. https://doi.org/10.1073/pnas.1013728107 (2010).

19. Herrera, J. E., Bergel, M., Yang, X. J., Nakatani, Y. & Bustin, M. The histone acetyltransferase activity of human GCN5 and PCAF is stabilized by coenzymes. *J. Biol. Chem.* **272**, 27253–27258. https://doi.org/10.1074/jbc.272.43.27253 (1997).

20. Glozak, M. A., Sengupta, N., Zhang, X. & Seto, E. Acetylation and deacetylation of non-histone proteins. *Gene* **363**, 15–23. https://doi.org/10.1016/j.gene.2005.09.010 (2005).

21. Kobayashi, T. et al. HDAC2 promotes loss of primary cilia in pancreatic ductal adenocarcinoma. *EMBO Rep.* **18**, 334–343. https://doi.org/10.15252/embr.201541922 (2017).

22. Mergen, M. et al. The nephronophthisis gene product NPHP2/Inversin interacts with Aurora A and interferes with HDAC6-mediated cilia disassembly. *Nephrol. Dial. Transpl. Off. Publ. Eur. Dial. Transpl. Assoc. Eur. Renal Assoc.* **28**, 2744–2753. https://doi.org/10.1093/ndt/gft316 (2013).

23. Yamauchi, T. et al. Distinct but overlapping roles of histone acetylase PCAF and of the closely related PCAF-B/GCN5 in mouse embryogenesis. *Proc. Natl. Acad. Sci. U. S. A.* **97**, 11303–11306. https://doi.org/10.1073/pnas.97.21.11303 (2000).

24. Tucker, R. W., Pardee, A. B. & Fujiwara, K. Centriole ciliation is related to quiescence and DNA synthesis in 3T3 cells. *Cell* **17**, 527–535. https://doi.org/10.1016/0092-8674(79)90261-7 (1979).

25. Fournier, M. et al. KAT2A/KAT2B-targeted acetylome reveals a role for PLK4 acetylation in preventing centrosome amplification. *Nat. Commun.* **7**, 13227. https://doi.org/10.1038/ncomms13227 (2016).

26. Xu, Z. et al. Microtubules acquire resistance from mechanical breakage through intralumenal acetylation. *Science* **356**, 328–332. https://doi.org/10.1126/science.aai8764 (2017).

27. Balasubramanyam, K. et al. Polyisoprenylated benzophenone, garcinol, a natural histone acetyltransferase inhibitor, represses chromatin transcription and alters global gene expression. *J. Biol. Chem.* **279**, 33716–33726. https://doi.org/10.1074/jbc.M402839200 (2004).

28. Pietrocola, F. et al. Spermidine induces autophagy by inhibiting the acetyltransferase EP300. *Cell Death Differ.* **22**, 509–516. https://doi.org/10.1038/cdd.2014.215 (2015).

29. Goldstein, L. S. & Yang, Z. Microtubule-based transport systems in neurons: The roles of kinesins and dyneins. *Ann. Rev. Neurosci.* **23**, 39–71. https://doi.org/10.1146/annurev.neuro.23.1.39 (2000).

30. Eshun-Wilson, L. et al. Effects of alpha-tubulin acetylation on microtubule structure and stability. *Proc. Natl. Acad. Sci. U. S. A.* **116**, 10366–10371. https://doi.org/10.1073/pnas.1900441116 (2019).

31. Keady, B. T. et al. IFT25 links the signal-dependent movement of Hedgehog components to intraflagellar transport. *Dev. Cell* **22**, 940–951. https://doi.org/10.1016/j.devcel.2012.04.009 (2012).

32. Malatesta, M. et al. Histone acetyltransferase PCAF is required for Hedgehog-Gli-dependent transcription and cancer cell proliferation. *Cancer Res.* **73**, 6323–6333. https://doi.org/10.1158/0008-5472.CAN-12-4660 (2013).

33. Chen, J. K., Taipale, J., Young, K. E., Maiti, T. & Beachy, P. A. Small molecule modulation of Smoothened activity. *Proc. Natl. Acad. Sci. U. S. A.* **99**, 14071–14076. https://doi.org/10.1073/pnas.182542899 (2002).

34. Deane, J. A. et al. Visualizing renal primary cilia. *Nephrology* **18**, 161–168. https://doi.org/10.1111/nep.12022 (2013).

35. Jensen, V. L. et al. Role for intraflagellar transport in building a functional transition zone. *EMBO Rep.* https://doi.org/10.15252/embr.201845862 (2018).

36. Jonassen, J. A., San Agustin, J., Follit, J. A. & Pazour, G. J. Deletion of IFT20 in the mouse kidney causes misorientation of the mitotic spindle and cystic kidney disease. *J. Biol.* **183**, 377–384. https://doi.org/10.1083/jcb.200808137 (2008).

37. Airik, R. et al. Renal-retinal ciliopathy gene Sdccag8 regulates DNA damage response signaling. *J. Am. Soc. Nephrol. JASN* **25**, 2573–2583. https://doi.org/10.1681/ASN.2013050565 (2014).

38. Cui, C. et al. Disruption of Mks1 localization to the mother centriole causes cilia defects and developmental malformations in Meckel-Gruber syndrome. *Dis. Models Mech.* **4**, 43–56. https://doi.org/10.1242/dmm.006262 (2011).

39. He, K. et al. Axoneme polyglutamylation regulated by Joubert syndrome protein ARL13B controls ciliary targeting of signaling molecules. *Nat. Commun.* **9**, 3310. https://doi.org/10.1038/s41467-018-05867-1 (2018).

40. Hong, S. R. et al. Spatiotemporal manipulation of ciliary glutamylation reveals its roles in intraciliary trafficking and Hedgehog signaling. *Nat. Commun.* **9**, 1732. https://doi.org/10.1038/s41467-018-03952-z (2018).

41. Dishinger, J. F. et al. Ciliary entry of the kinesin-2 motor KIF17 is regulated by importin-beta2 and RanGTP. *Nat. Cell Biol.* **12**, 703–710. https://doi.org/10.1038/ncb2073 (2010).

42. Milic, B., Andreasson, J. O. L., Hogan, D. W. & Block, S. M. Intraflagellar transport velocity is governed by the number of active KIF17 and KIF3AB motors and their motility properties under load. *Proc. Natl. Acad. Sci, U. S. A.* **114**, E6830–E6838. https://doi.org/10.1073/pnas.1708157114 (2017).

43. Li, G. et al. A role for Alstrom syndrome protein, alms1, in kidney ciliogenesis and cellular quiescence. *PLoS Genet.* **3**, e8. https://doi.org/10.1371/journal.pgen.0030008 (2007).

44. Lu, H. et al. Mutations in DZIP1L, which encodes a ciliary-transition-zone protein, cause autosomal recessive polycystic kidney disease. *Nat. Genet.* **49**, 1025–1034. https://doi.org/10.1038/ng.3871 (2017).

45. Yu, F., Sharma, S., Skowronek, A. & Erdmann, K. S. The serologically defined colon cancer antigen-3 (SDCCAG3) is involved in the regulation of ciliogenesis. *Sci. Rep.* **6**, 35399. https://doi.org/10.1038/srep35399 (2016).

46. Bowie, E., Norris, R., Anderson, K. V. & Goetz, S. C. Spinocerebellar ataxia type 11-associated alleles of Ttbk2 dominantly interfere with ciliogenesis and cilium stability. *PLoS Genet.* **14**, e1007844. https://doi.org/10.1371/journal.pgen.1007844 (2018).

Acknowledgements

Author contributions

J. H. Park and K. H. Yoo: Conceptualization. H. Cha, J.Y. Ko, and Ho-S. Kim: Methodology. H. Cha, J. H. Jun, J. Y. Ko: Formal analysis and investigation. H. Cha and J. H. Jun: Writing—original draft preparation. H. Cha, J. H. Jun, J. Y. Ko, and J. H. Park: Writing—review and editing. J. H. Park: Funding acquisition. Ho-S. Kim: Resources. J. H. Park: Supervision.

Declarations

Competing interests

The authors declare no competing interests.

Additional information

Supplementary Information The online version contains supplementary material available at https://doi.org/1 0.1038/s41598-025-86292-5.

Correspondence and requests for materials should be addressed to K.H.Y. or J.H.P.

Reprints and permissions information is available at www.nature.com/reprints.

Publisher's note Springer Nature remains neutral with regard to jurisdictional claims in published maps and institutional affiliations.